Shrestha, M, Steele, IA, Piascik, AS, Jermak, HE, Smith, RJ and Copperwheat, CM

 Characterization of a dual-beam, dual-camera optical imaging polarimeter

http://researchonline.ljmu.ac.uk/id/eprint/12835/

Article

For more information please contact researchonline@ljmu.ac.uk

Characterization of a dual-beam, dual-camera optical imaging polarimeter

Manisha Shrestha ●,★ Iain A. Steele, Andrzej S. Piascik, Helen Jermak, Robert J. Smith and Chris M. Copperwheat

Astrophysics Research Institute, Liverpool John Moores University, Liverpool Science Park IC2, 146 Brownlow Hill, Liverpool L3 5RF, UK

ABSTRACT

Polarization plays an important role in various time-domain astrophysics to understand the magnetic fields, geometry, and environments of spatially unresolved variable sources. In this paper we present the results of laboratory and on-sky testing of a novel dual-beam, dual-camera optical imaging polarimeter (MOPTOP) exploiting high sensitivity, low-noise CMOS technology, and designed to monitor variable and transient sources with low systematic errors and high sensitivity. We present a data reduction algorithm that corrects for sensitivity variations between the cameras on a source-by-source basis. Using our data reduction algorithm, we show that our dual-beam, dual-camera technique delivers the benefits of low and stable instrumental polarization (<0.05 per cent for lab data and <0.25 per cent for on sky data) and high throughput while avoiding the additional sky brightness and image overlap problems associated with dual-beam, single-camera polarimeters.

Key words: instrumentation: polarimeters.

1 INTRODUCTION

The polarization state of light can provide complementary knowledge of the source to that we can infer from other techniques such as photometry, spectroscopy, and imaging. Thus, we are losing valuable information when we ignore the polarization of different astrophysical sources. Polarimetry has proven to be a powerful diagnostic tool for various science cases such as studying environment around stellar sources (Brown & McLean 1977; Shrestha et al. 2018), supernovae remnants (Hoffman et al. 2008), blazars (Jermak 2017), gamma-ray bursts (GRBs; Steele et al. 2009; Mundell et al. 2013), novae (Harvey et al. 2018), and many more. In recent years polarimetric studies have taken a leading role as a key diagnostic tool of magnetic field strength/order/geometry, geometry of environment surrounding the source, and relativistic plasma dynamics in various time domain sources such as blazars, active Galactic nuclei, x-ray binaries, and GRBs. Polarization studies of these time varying sources can provide spatial resolution information not possible by other techniques.

Optical polarization is traditionally measured via a ratio of fluxes in two or more polarization states obtained consecutively. This approach does not work for rapidly fading targets such as GRBs where an erroneous signal can be introduced due to rapid fluctuation in flux. To address this problem we developed a series of polarimeters (RINGO, RINGO2, and RINGO3) that used a rapidly rotating polaroid analyser (Arnold 2017; Jermak 2017) on the 2.0-

m Liverpool Telescope (LT). These instruments have successfully observed various time varying sources. RINGO2 was used to make first ever detection of early-time optical polarization in GRBs (Steele et al. 2009). Mundell et al. (2013) observed high polarization of a GRB and its time evolution using RINGO2. RINGO2 and RINGO3 have also been used to produce a comprehensive multicolour polarization data set of blazar variability (Jermak et al. 2016a).

Multicolour OPTimised Optical Polarimeter (MOPTOP) is the next generation of polarimeter to replace RINGO3 at the Liverpool Telescope. MOPTOP benefits from the advantages of the RINGO series of instruments such as a fast rotating element to allow high time resolution and the use of fast readout, very low noise cameras. In addition, it uses a unique optical dual-camera configuration to minimize systematic errors and provide the highest possible sensitivity. Dual-beam polarimeters have been built before e.g. Scarrott et al. (1983), however they often combine the signal on to a single camera because traditionally the imaging detector has been the most expensive component. This combining causes problems such as source overlap and reduced sensitivity via increased sky background. The recent availability of relatively low cost scientific complementary metal-oxide semiconductor (sCMOS) detectors with high quantum efficiency, very low read noise, and rapid readout, means a dual camera imaging polarimeter becomes feasible.

In this paper we will characterize a prototype version of MOPTOP and show that a dual-beam, dual-camera polarimeter indeed has better polarimetric accuracy and sensitivity. We will also describe a data analysis algorithm for dual-camera data that will be available for future MOPTOP science observations. The paper is organized as

★ E-mail: ms1228@truman.edu
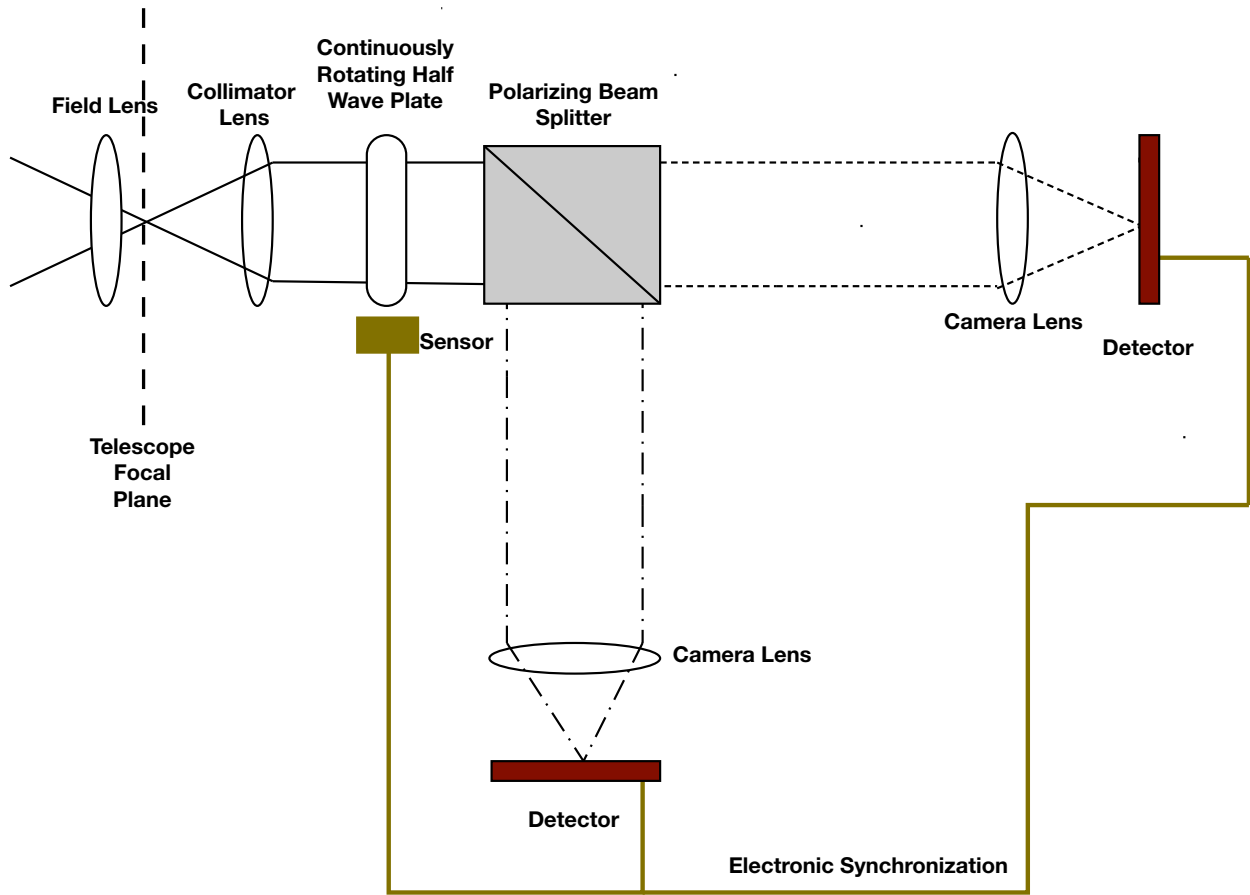
Figure 1. Layout of MOPTOP illustrating the design principal and major components from Jermak, Steele & Smith (2016b). The solid black line represents the incoming light from source. It passes through a field lens, a collimator lens, and a continuously rotating half wave plate which modulates the polarization angle of the incoming beam. This beam is split into *s* and *p* represented by the dashed and dot-dashed lines. Both polarization states are simultaneously recorded by fast readout sCMOS cameras synchronized to the wave plate angle.

follows. In Section 2, we provide the design of the instrument and its features. Section 3 provides the steps of the data reduction pipeline that can be employed to reduce MOPTOP data. We provide details of data observed from lab and on-sky observations in Section 4. Then we present the results of these observed data in Section 5 and provide concluding remarks in Section 6.

2 MOPTOP POLARIMETER

Conceptually, MOPTOP is a fully optimized polarimeter for time-domain astrophysics. As such it was designed to meet the following key requirements:

(i) Maximum sensitivity for faint sources.

(ii) Low systematic errors allowing measurements of low polarization sources.

(iii) Ability to measure a rapidly variable or fading source.

(iv) Ability to measure all sources in a wide field of view without source overlap or prior identification.

(v) Ability to measure sources over the widest possible dynamic range of photon counts.

The full design concept is explained in detail in Jermak et al. (2016b) and the optical design and results of ray-tracing are presented in Jermak, Steele & Smith (2018). MOPTOP is a dual-

beam, dual-camera polarimeter which uses two sCMOS cameras per waveband as detectors. The full concept includes an inline filter wheel to provide simultaneous multiband capability, however, for this paper we present the results of testing a simpler single band version of the instrument.

The advantages of a dual-beam approach to polarimetry have long been known (e.g. Clarke 1965) in that it allows cancellation of the systematic errors that arise in simple single-beam polarimetry. Key to the technique is the use of a half wave plate to modulate the polarization angle of the incoming beam and an analyser system that can simultaneously record the two orthogonal polarization states. A rotation of the wave plate by 22.5° will rotate the polarization angle of the beam by 45°, effectively swapping the *q* and *u* Stokes parameters. This means that variations in the polarization response of the instrument can be corrected by a differential technique and gives the consequent reduction in systematic errors.

A sketch of our single band version is presented in Fig. 1. The design was implemented using off-the-shelf optical elements, cameras and mechanical components housed within a set of lens tubes. These were then supported by a custom aluminium chassis to interface with the telescope. Briefly the key elements of the implementation are:

(i) An input filter (not shown) that defines the instrument wavelength range. This is a custom filter comprised of 3-mm Schott
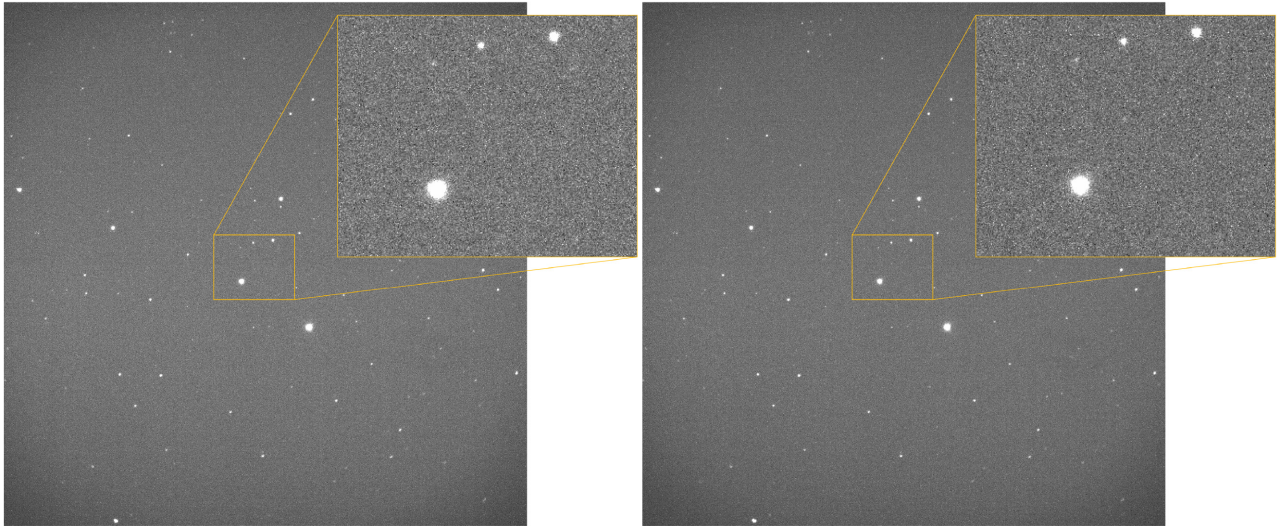
Figure 2. Raw image of star field SA111-14 (Landolt 2009) observed by one CMOS camera at two consecutive waveplate positions. The images show slight vignetting in the field corners due to the optical system. The zoomed portions of the image show both static dark frame ('hot pixel') and flat-field structures and the presence of random telegraph ('popcorn') noise apparent as 'hot pixels' that appear in random locations from frame to frame.

GG475 glass cemented to 2-mm Schott KG3 that was originally used in the RINGO 1 and 2 polarimeters. It gives an approximate wavelength range of 4750–7100 Å (FWHM = 2350 Å), and as we showed in Steele et al. (2017), provides a good photometric match to the Sloan r' band.

(ii) An achromatic field ($f = 300$-mm) and collimator ($f = 150$-mm) lens combination that collimates the output beam from the telescope and places the pupil to coincide with the position of the beam splitter. Both lenses have an antireflection coating with $R < 1$ per cent per surface between 4000 and 10 000 Å.

(iii) A Thor Labs achromatic half-wave plate which rotates to modulate the polarization angle of the incoming beam. This has 98 per cent transmission (including the effect of antireflection coatings) and a retardance within 0.02λ of the ideal $\lambda/2$ over the wavelength range defined by the input filter. The wave plate is mounted in a Physik Instrumente model U-651 rotation stage that in normal operation is continuously rotated at 7.5 revolutions per minute.

(iv) A Thor Labs high-throughput polarizing wire-grid beam splitter with 4000–7000 Å antireflection coating and a contrast ratio $> 1000{:}1$ for angles of incidence between 0 and 25° over that wavelength range. This separates the beam into *s* and *p* polarization states to be recorded on two separate cameras.

(v) A pair of Nikon SLR camera lenses (50-mm, *f*/1.4) to focus the collimated *s* and *p* beams on to the detectors.

(vi) A pair of Andor Zyla 4.2 sCMOS detectors with 2048×2048 pixels and yielding a field of view of $\sim 7 \times 7$ arcmin. The cameras are specified to have rapid readout (< 0.01-s), very low read noise ($< 1\ e^-$), and high quantum efficiency (~ 80 per cent). Readout of the detectors is electronically synchronized to each other and the angle of the wave plate rotation stage using its inbuilt encoder to generate a hardware trigger signal to the cameras (Steele et al. 2016). An example of two consecutive raw images from one detector is presented in Fig. 2.

(vii) Two compact Intel NUC PCs with Intel i7 processors and M.2 solid state drives running Linux Ubuntu 18.04. The computers are mounted either side of the instrument housing and separately acquire images from each camera over a USB 3.0 interface. One of the PCs also controls the half-wave plate rotator stage and could control a filter wheel in a future upgraded instrument.

At low levels of polarization, the sensitivity of a polarimeter will be dominated by systematic effects. These are hard to predict, however as described above, the dual-beam dual-camera design of MOPTOP aims to minimize these. As a comparison, the single beam, single-camera RINGO series of polarimeters have suffered systematic effects at the ~ 0.5 per cent level (Słowikowska et al. 2016). For higher degrees of polarization, polarization sensitivity may be calculated via simple photon statistics, taking into account the sky-brightness and source fluxes (including the system throughputs and detector quantum efficiencies) and detector read-noises. The results of such a calculation for RINGO3 and MOPTOP are presented in Fig. 3. This shows (for example) that a 100 s exposure with MOPTOP on an $R = 17$ magnitude object is predicted to attain a polarization accuracy of ~ 0.6 per cent, compared to the RINGO3 value of ~ 2.6 per cent. There are two principal reasons for this improvement. First there will be a doubling of photon throughput from switching from a Polaroid (which blocks half of the flux) to a beam-splitter arrangement. Secondly there will be an effective doubling of detector quantum efficiency by moving from EMCCD detectors, which suffer from multiplicative noise in their gain stage (Robbins & Hadwen 2003), to sCMOS.

3 DATA REDUCTION PIPELINE

Data taken with MOPTOP produces 16 different images from each camera, with each image frame corresponding to a 22.5° rotation of the wave-plate (Fig. 4). These data can be reduced in two different ways to get polarization values. Common to both methods is the use of aperture photometry to extract sky-corrected source counts. The extracted counts can then be converted to fractional Stokes parameters *q-u* via two different techniques which we call 'one-camera' and 'two-camera'. In the one-camera technique we use fluxes from eight frames from one camera to calculate fractional Stokes parameters *q-u* following the recipe of Clarke & Neumayer (2002). These Stokes parameters can then be used to calculate polarization degree and angle.
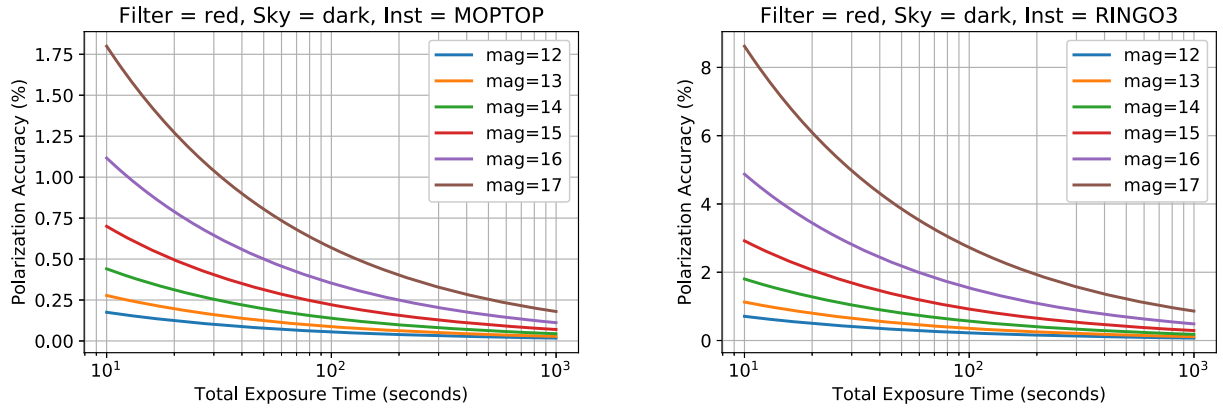
Figure 3. Predicted polarization accuracy with respect to total exposure times for a range of magnitudes represented by different colours. The left-hand side figure is for MOPTOP and the right-hand side figure is for RINGO3 both for dark sky and magnitude 21.5 in *R* band filter. The x-axis is in a logarithmic scale for both cases.
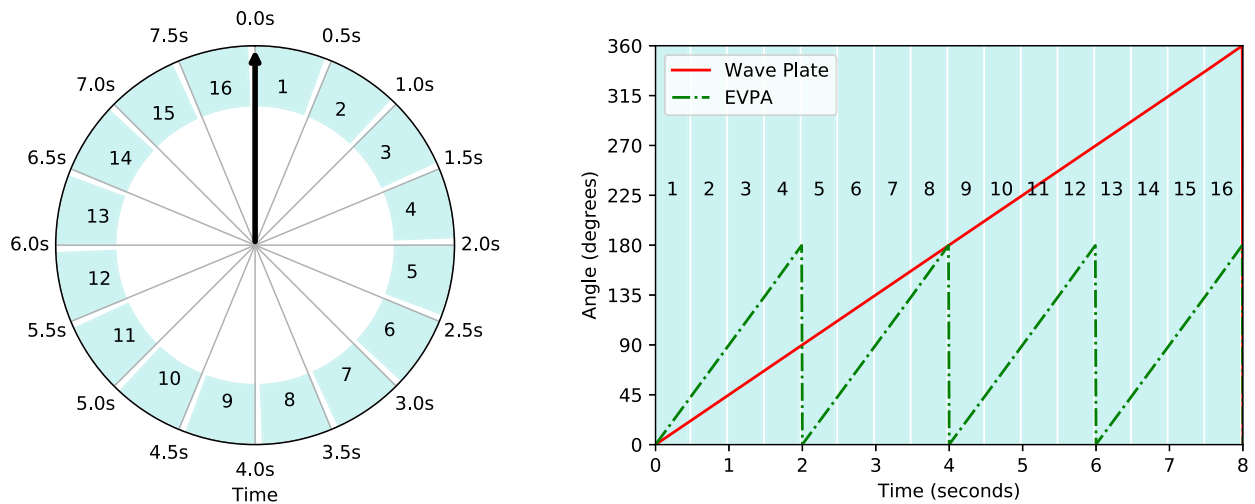
Figure 4. Left-hand panel: MOPTOP operational principle, showing the sequence of frames taken at different angles of the rotating wave plate as a function of time. Exposure of a frame simultaneously begins on both cameras 0.5 s after the previous one, with the waveplate rotation angle having increased by a total of 22.5 degrees over that time period. The blue shaded areas indicate the time the shutter is open (duration 0.45 s), with the shorter white regions indicating the 0.05 s readout gaps between frames. Frames are numbered 1-16, corresponding to the notation introduced in Section 3.2. Right-hand panel: Waveplate rotation angle and resulting EVPA rotation of the incoming beam as a function of time.

In the two-camera technique we make use of all 16 frames from both cameras. The beam splitter in MOPTOP separates the incoming beam into *s* and *p* polarization states which are recorded on two cameras. Because of the presence of the rotating half wave plate, the difference between the two camera images at the first half wave plate position of 0° equals the Stokes Q parameter and the difference at half wave plate position of 22.5° equals the Stokes U parameter. The subsequent third half wave plate position difference yields -Q and the fourth -U. The sum of all the fluxes from four half wave plate position divided by 2 gives the Stokes parameter I.

3.1 Flux extraction

We perform aperture photometry using the Python package AS-TROPY PHOTUTILS (Bradley et al. 2019). Depending on the source, we use either global background subtraction (when there is a source close to the target) or local background subtraction (when there is no source close to the target). For global background, we estimate the background using a median of the whole image via sigma clipped statistics in ASTROPY (Price-Whelan et al. 2018). We subtract the global median as the background signal. For local background estimate we use an annulus aperture to estimate the background signal and subtract it from the source. After background subtraction we detect sources above 5 to 15 times the standard deviation of the image signal-to-noise (SNR) using DAOStarFinder which provides x and y coordinates of the sources in pixel values.

In order to calculate appropriate aperture size to perform aperture photometry, we check the full width at half-maxium (FWHM) of the source as well as how magnitude and error in magnitude changes with aperture size. We use the combination of these two techniques i.e. an aperture size between 2 to 3 times FWHM and that produces good SNR as the appropriate aperture size. This aperture size around the sources is used to perform aperture photometry and calculate the counts from all the sources. At the end of the routine we have counts values for the sources with a certain threshold SNR for all the 16 frames required for polarization calculations. Along with counts we also calculate the error in these counts which is the root mean square sum of background noise and Poisson noise of the source (Bradley et al. 2019). The values we get from photometry are used to calculate the polarization of the sources.

3.2 One-camera technique

In our one-camera technique we implement the procedure outlined by Clarke & Neumayer (2002). This is also the procedure we used for RINGO, RINGO2, and RINGO3 data reduction (e.g. Jermak et al. 2016a). In this method the data from one camera for eight consecutive rotor frames are used to calculate the Stokes parameters. The observed photoelectron-counts for an object in each frame are given by m_n where n represents the frame number (Fig. 4). These photoelectron-counts are then used to calculate the quantities S_1, S_2, and S_3:

$$S_1 = m_1 + m_2 + m_3 + m_4 + m_5 + m_6 + m_7 + m_8, \tag{1}$$

$$S_2 = m_1 + m_5 + m_2 + m_6, \tag{2}$$

$$S_3 = m_2 + m_6 + m_3 + m_7. \tag{3}$$

S_1, S_2, and S_3 can then be used to calculate the Stokes parameters q and u using the Clarke & Neumayer (2002) equations:

$$q = \frac{Q}{I} = \pi \left(\frac{1}{2} - \frac{S_3}{S_1} \right), \tag{4}$$

$$u = \frac{U}{I} = \pi \left(\frac{S_2}{S_1} - \frac{1}{2} \right). \tag{5}$$

Using the Stokes parameters q and u, we can then calculate the polarization degree (p) and polarization angle (ψ):

$$p = \sqrt{q^2 + u^2}, \tag{6}$$

$$\psi = \frac{1}{2} \arctan \left(\frac{u}{q} \right). \tag{7}$$

In equation (7) we take care to determine the correct quadrant for ψ.

Errors can be calculated using the photoelectron-count errors as follows:

$$S_{1e} = \sqrt{m_{1e}^2 + m_{5e}^2 + m_{2e}^2 + m_{6e}^2 + m_{3e}^2 + m_{7e}^2 + m_{4e}^2 + m_{8e}^2}, \tag{8}$$

$$S_{2e} = \sqrt{m_{1e}^2 + m_{5e}^2 + m_{2e}^2 + m_{6e}^2}, \tag{9}$$

$$S_{3e} = \sqrt{m_{2e}^2 + m_{6e}^2 + m_{3e}^2 + m_{7e}^2}, \tag{10}$$

where subscript 'e' denotes the error in corresponding measurements. We then do error propagation in equations (4) and (5) to calculate the error in corresponding Stokes parameters:

$$q_e = \pi \sqrt{\left(\frac{s_{3e}}{s_1} \right)^2 + \left(\frac{s_{1e} s_3}{s_1^2} \right)^2}, \tag{11}$$

$$u_e = \pi \sqrt{\left(\frac{s_{2e}}{s_1} \right)^2 + \left(\frac{s_{1e} s_2}{s_1^2} \right)^2}. \tag{12}$$

Finally we use the Monte Carlo technique of Steele et al. (2017) which is based on Simmons & Stewart (1985) to correct for polarization bias and calculate the error in polarization degree and position angle from the errors in q and u.

3.3 Two-camera technique

The one-camera technique described in Section 3.2 is similar to the technique we use with RINGO3. The novel technique of the MOPTOP dual-beam polarimetry is properly utilized when we reduce the polarization values using a two-camera technique. As described in Section 3, we can take the difference between two

cameras at various half-wave plate angles to get Stokes Q, U, -Q, and -U. To do this we need to ensure the observed counts from the two different cameras have the same effective sensitivity. This is unlikely to be true by default, as the two beams and cameras will have slightly different flat-field and quantum efficiency characteristics.

For each individual source in a set of images, we define the quantity F ('the sensitivity factor') as the ratio of counts between camera 2 and camera 1 for an unpolarized source at a certain location on the camera. We then define m_1 and n_1 as the observed counts from camera 1 and camera 2 respectively for half-wave plate angle $0°$ (Fig. 4). We then define c_1 and d_1 as the counts after correction for the difference in sensitivity. Hence $c_1 = m_1$ and $d_1 = \frac{n_1}{F}$. We can calculate Stokes Q as $c_1 - d_1$ and Stokes I as $c_1 + d_1$, hence we can calculate fractional q as:

$$q = \frac{Q}{I} = \frac{c_1 - d_1}{c_1 + d_1}. \tag{13}$$

Substituting to the counts observed

$$q = \frac{Q}{I} = \frac{m_1 - n_1/F}{m_1 + n_1/F}. \tag{14}$$

Similarly the counts of camera 1 and camera 2 at $22.5°$ can be written as c_2 and d_2 respectively which can be converted to observed counts as $c_2 = m_2$ and $d_2 = \frac{n_2}{F}$ And the counts of camera 1 and camera 2 at $45°$ can be written as c_3 and d_3 respectively which can be converted to observed counts as $c_3 = m_3$ and $d_3 = \frac{n_3}{F}$.

The difference in this counts give us Stokes -q

$$-q = \frac{Q}{I} = \frac{m_3 - n_3/F}{m_3 + n_3/F}. \quad q = \frac{n_3 - m_3/F}{n_3 + m_3/F}. \tag{15}$$

We can equate equation (14) and the negative of equation (15), which gives us

$$F = \sqrt{\frac{n_1 n_3}{m_1 m_3}}. \tag{16}$$

We can therefore calculate the sensitivity factor F for all the eight pairs of subsequent frames. We use each F factor calculated for a pair to correct for the counts corresponding to those frames. Finally these corrected counts are utilized to calculate the Stokes q (equation 14) and u via:

$$u = \frac{U}{I} = \frac{m_2 - n_2/F}{m_2 + n_2/F}. \tag{17}$$

We then take the average of two consecutive Stokes q and u to get our final Stokes q and Stokes u from a set of four images. These q and u values calculated via the two camera technique can be used in equations (6) and (7) to calculate the polarization degree and position angle, respectively.

We use the error propagation in equations (14) and (17) to calculate the error in Stokes q and u respectively:

$$q_e = \sqrt{n_{1e}^2 + (((m_3/(2n_1 n_3 m_1))^2 \times (1/(n_1 n_3 m_1)^2) \times}$$
$$\sqrt{((n_{1e}/n_1)^2 + (n_{3e}/n_3)^2 + (m_{1e}/m_1)^2)) + (m_{3e}/m_3)^2)}. \tag{18}$$

$$u_e = \sqrt{n_{2e}^2 + (((m_4/(2n_2 n_4 m_2))^2 \times (1/(n_2 n_4 m_2)^2) \times}$$
$$\sqrt{((n_{2e}/n_2)^2 + (n_{4e}/n_4)^2 + (m_{2e}/m_2)^2)) + (m_{4e}/m_4)^2)}, \tag{19}$$

where subscript 'e' is the error in the corresponding measurement.
Again we use the Monte Carlo technique as per Section 3.2 to calculate the error in polarization degree and position angle.

Table 1. Targets observed by MOPTOP on 2019 Sept 8 – 10 at LT.

Name	RA (J2000)	Dec. (J2000)	R mag	Comments
BD +32 3739	20 12 02.11	+32 47 43.5	9.3	Unpolarized Standard
BD +28 4211	21 51 11.07	+28 51 51.8	10.5	Unpolarized Standard
HD 212311	22 21 58.55	+56 31 52.8	8.12	Unpolarized Standard
HILT 960	20 23 28.53	+39 20 59.1	10.6	Polarized Standard
VICyg 12	20 32 40.94	+41 14 26.2	11.5	Polarized Standard
HD 204827	21 28 57.70	+58 44 24.0	7.94	Polarized Standard
KIC 8462852	20 06 15.4	+44 27 24.7	11.75	Boyajian et al. (2016)

4 DATA

To study MOPTOP's initial performance, data were collected in the lab (see Section 4.1) and polarized and unpolarized standard stars were observed on sky (see Section 4.2) using the LT.

4.1 Laboratory testing

The instrument was setup in the lab to test the basic polarization performance without the influence of the telescope optics. We aimed to simulate three different light sources: unpolarized (~ 0 per cent), partially polarized ($4 - 5$ per cent), and highly polarized (~ 100 per cent).

In order to simulate an unpolarized light source we experimented with both incandescent bulb and LED light sources, eventually arriving at array of five white-light LEDs arranged with their intrinsic polarizations in a radial pattern. This was used to illuminate a domestic sucrose sugar-cube which acted as a polarization scrambler before the light was fed via a 10-m length of multi-mode optical fibre which further scrambled the polarization and produced a small, bright source at its output that acted as an artificial star. To create a partially polarized source, the output from the artificial star was then reflected at 45° from a front-surface aluminium mirror. This should produce a polarization of 4–5 per cent (Cox 1976). Finally an off-the shelf Polaroid sheet was used to produce a highly polarized source option.

These sources were observed using MOPTOP and the polarization of the sources was calculated following the data reduction pipeline described in Section 3. Results are presented in Section 5.

4.2 Observations on sky

MOPTOP was mounted on the 2.0-m fully robotic Liverpool Telescope (Steele et al. 2004) in the Roque de Los Muchachos Observatory, La Palma, Spain for three days of observations from 2019 September 8 to 2019 September 10. MOPTOP on LT yielded a field of view of 7×7 arcmin ($4 \times$ greater than the RINGO series of instruments). The sCMOS detector gains were set at $0.55e^-/ADU$ with a median read noise of $0.9e^-$.

For the three nights of observations, we selected various standard polarized and unpolarized stars whose polarization degree is available in literature. For the better understanding of instrument performance, we varied various parameters like the Cassegrain rotator angle, star field, and varying magnitude of the targets. The list of observed targets are presented in Table 1.

5 RESULTS

Following an initial confirmation of camera linearity via observations of the standard field SA111-SF2 (Landolt 2009), we analysed our laboratory and on sky data using the data reduction pipeline described in Section 3. The following subsections present our polarization results and show that our dual-beam, dual-camera polarimeter produces better polarization accuracy and sensitivity than our previous single-camera, single beam designs.

5.1 One-camera technique versus two-camera technique

First as a proof of concept we checked how the two-camera technique compared to the one-camera technique. We reduced all the 16 frames of data for each camera and implemented the data reduction pipeline as described in Section 3. From each technique, we get four different Stokes q and u parameters. We calculated polarization degree and error in polarization degree.

Fig. 5 shows how error in polarization degree varies with electron counts (left-hand panel) and magnitude (right-hand panel) for the one-camera and two-camera techniques for MOPTOP observations and RINGO3 observations. We can see that the two-camera technique has the lowest error in polarization degree compared to the other two techniques which is expected as the two-camera technique makes use of all the photons observed whereas the one-camera and RINGO3 techniques only use half of the photons detected by the instrument. We can also compare the results in Fig. 5 from observations with results in Fig. 3 from simulations. We find that the observed error in polarization degree is close to the simulated error in polarization degree. For example, the 12th magnitude star with ~ 6 s exposure time has 0.289 per cent error in polarization degree from observations and from simulations the expected error in polarization degree is 0.226 per cent.

Another way to compare the two techniques was to look at standard deviation in different Stokes q values for the one-camera and two-camera techniques for different sources. Fig. 6 presents standard deviation in Stokes q for eight different values (first four are from one-camera technique and last four are from two-camera technique) we get from MOPTOP observations. We can see for all the sources observed, the two-camera technique has less scatter in Stokes q compared to the one-camera technique. Thus, showing that the two-camera technique has less systematic error compared to the one-camera technique. As expected we see the same behaviour for Stokes u.

These comparisons show that the two-camera technique produces better results with less error in polarization degree and less scatter in Stokes q and u compared to the one-camera technique. For the rest of the results sections we therefore only present the two-camera technique for clarity unless stated otherwise.

5.2 Laboratory data results

Our laboratory test data was analysed using the two-camera technique to calculate polarization degree to characterize the instrument before on-sky observations. Fig. 7 includes the results of
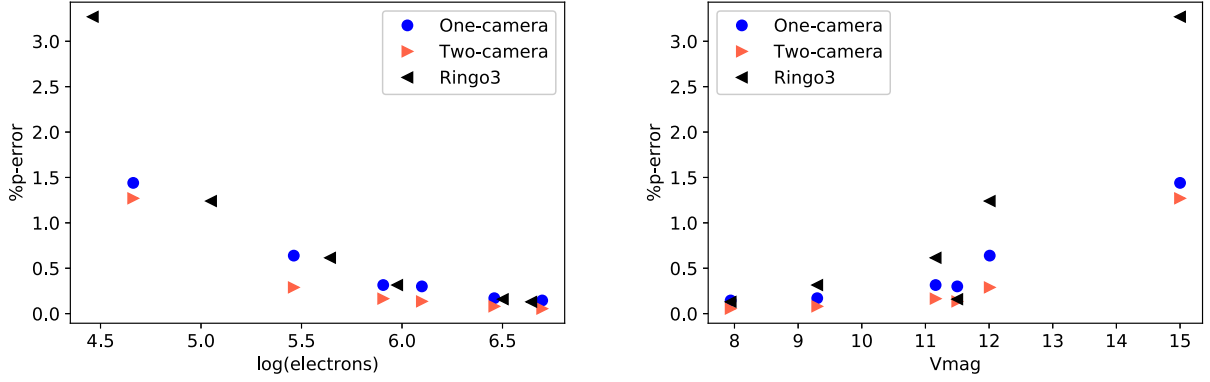
Figure 5. Calculated formal errors (derived from equations 11, 12, 18, 19) in polarization degree for equal length integration times with MOPTOP and RINGO3 of the Landolt field SA111-SF2. The blue circles represent results from MOPTOP one-camera technique, red triangles are for the two-camera MOPTOP technique, and black triangles for data from RINGO3. The left-hand figure is plotted with respect to the total number of photo-electrons recorded and shows similar polarization accuracy for RINGO3 and the single camera analysis of MOPTOP. The advantage of the two-camera MOPTOP technique is clear. The right-hand figure shows polarimetric error as a function of source magnitude, and demonstrates the throughput advantage of MOPTOP even in one camera mode.

the observed polarization degree for various sources. For our unpolarized source, the mean of all the observed polarization degrees is 0.24 per cent and the standard deviation is 0.054. While it is possible that the laboratory source is not fully unpolarized, this shows that the intrinsic polarization of the instrument must be less than that value.

For the partially polarized source we found a mean of 3.7 per cent with a standard deviation of 0.106. This is in line with expectations (4 − 5 per cent), and the low standard deviation indicates that systematic errors are likely to be low.

Finally for our fully polarized source, we get a mean of 95.23 per cent and standard deviation of 0.245. Given the source is likely not-fully polarized due to the limited contrast ratio of off-the-shelf Polaroid, we can use this result to establish an upper limit to any instrumental depolarization of <5 per cent of the measured value.

Overall these results show that instrument is working as expected and introduces a very low level of instrumental polarization and depolarization in the case where there is no background noise and no additional polarization from mirrors of the telescope.

5.3 Unpolarized standard stars

The first three stars in Table 1 are unpolarized standards we observed during the observation run. The archival data show that these stars are unpolarized and the values are presented in Table 2. BD+323739 and BD+284211 were observed with exposure time per frame 0.46 s and HD212311 was observed with exposure time per frame 0.2 s. We varied Cassegrain rotor angles ranging from −90° to +90° with an increment of 22.5°. We observed these stars for two nights in a row. In Table 2, we present the observed polarization degree compared to catalogue values for these stars.

For the observed data, we used the two-camera technique to reduce the data and obtained Stokes q, u and errors in q and u. We find there is a smaller scatter in Stokes q and u for these stars from MOPTOP observations compared to those seen from RINGO3 observations (Słowikowska et al. 2016). We present the results of observed unpolarized standard stars in Figs 8 and 9. For BD+323739, BD+284211, and HD212311, we find q_{avg} = 0.0056, 0.0080, 0.01570, respectively and standard deviation q_{std} = 0.00105, 0.00273, 0.00126, respectively. For Stokes u the
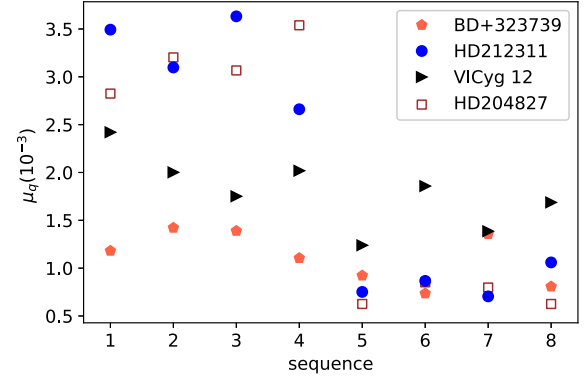

Figure 6. Standard deviation in Stokes q with respect to different sequences of observations for different stars observed. First four sequences are for one-camera technique and last four are for two-camera technique.

averages are, u_{avg} = −0.0245, −0.0211, −0.0211, respectively and standard deviations are u_{std} = 0.00097, 0.00265, 0.001706, respectively as shown in Figs 8 and 9. These values are calculated for all the observed data taken during observational run and averaged over four different Stokes parameters we get from the two-camera technique. As these are unpolarized standard stars, we expect Stokes q and u to be zero. We see that the mean of Stokes q depends on exposure time since this will be related to the mean wave plate angle during an exposure. Thus, we get different average Stokes q for HD212311 which had half the exposure time of other two unpolarized standard stars. Hence the average from each star is considered as the additional polarization introduced by the instrument, dependent on exposure time.

5.4 Polarized standard stars

The next three stars in Table 1 i.e. Hilt 960, VICyg 12, and HD 204827 are polarized standard stars we observed using MOPTOP on the LT during its commissioning run. These targets are relatively highly polarized and have good archival data as presented in Table 2. Hiltner 960 and VICyg 12 were observed with exposure
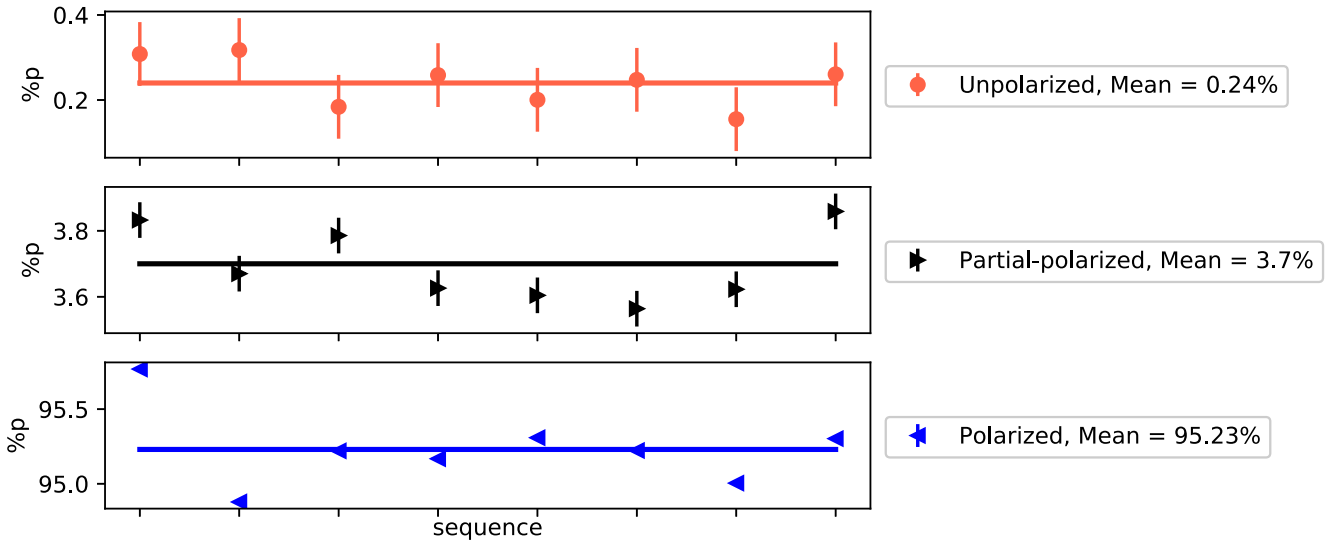
Figure 7. Polarization degree for different set of laboratory data. The three panels are for simulated light in the lab of unpolarized light (~ 0 per cent), partially polarized light ($4 - 5$ per cent), and fully polarized light (~ 100 per cent) for top panel, middle panel, and bottom panel respectively. The points represent data points from observation and the solid line represents the mean of the data points. Error in polarization degree is shown by the vertical solid line. The label consists of mean value for each panel.

Table 2. Polarimetric archival data of the polarized and unpolarized standard stars along with data from MOPTOP observation for R band before correcting (Uncor) for instrumental polarization and after corrected (Cor). Errors are calculated using the Monte Carlo technique described in Section 3. Polarimetric archival data from Schmidt, Elston & Lupie (1992) for the unpolarized (in V band) and polarized (in R band) standard stars. The catalogue polarization value for KIC 8462852 is from Steele et al. (2018) for R band.

| | | Obs percent p | |
Name	Cat percent p	Uncor	Obs percent p Cor
BD +32 3739	0.025 ± 0.017	2.513 ± 0.080	–
BD +28 4211	0.054 ± 0.027	2.245 ± 0.080	–
HD 212311	0.034 ± 0.021	2.620 ± 0.075	–
HILT 960	5.210 ± 0.029	–	–
VICyg 12	7.893 ± 0.037	6.840 ± 0.129	6.965 ± 0.129
HD 204827	4.893 ± 0.029	4.673 ± 0.064	4.755 ± 0.064
KIC 8462852	0.6 ± 0.1	2.273 ± 0.280	0.750 ± 0.280

time 0.46 s per frame and HD 204827 was observed with exposure time 0.2 s per frame.

We used the data reduction pipeline as discussed in Section 3 to reduce the polarized standard star data. Results for only two of the polarized standard stars observed are presented in Figs 10 and 11 because we observed Hiltner 960 at different Cassegrain rotor position for the first night and the data quality for that day is not on the par with other observations. The blue points represent the observed Stokes q-u values for different Cassegrain rotor positions before correcting for instrumental polarization. The dashed blue lines represent the best fit for observed data and the solid black line is the catalogue value. The red cross shows the centre of the best-fitting circle for the observed data points. For corrected values, the circle should centre on the origin. In both cases, the red triangle represent data after they were corrected for instrumental polarization using unpolarized standard stars. For red points in Fig. 10, we use results from BD +28 4211 ($q_{inst} = 0.008$ and $u_{inst} = -0.021$) as our instrumental polarization because both have same exposure time. For Fig. 11 we use results from HD 212311 ($q_{inst} = 0.0157$ and u_{inst}
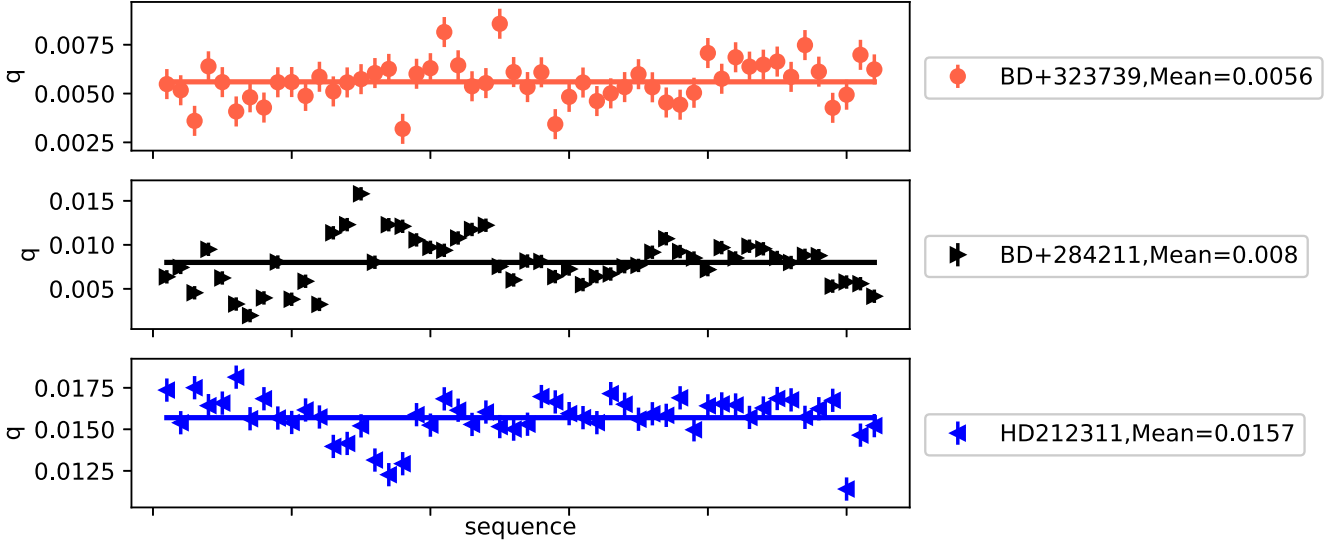
$= -0.0211$) as instrumental polarization for correction because both have same exposure time.

After the correction, the centre of the data moves closer to the origin and the best-fitting circle of dashed red line is more circular and more closely matched to the solid black circle created using catalogue values. The observed value for HD 212311 after correction for instrumental polarization is close to the catalogue values as seen in Fig. 11. However for VICyg 12 the match is not as good between observed and catalogue values as can be seen in Fig. 10. For VICyg 12 we see apparent significant ($\sim$15 per cent) depolarization in observed values compared to the catalogue value. The difference between these two objects means we cannot comment definitively on on-sky instrumental depolarization based on this data set alone. However we note that we did not see evidence for strong instrumental polarization in our laboratory data. We also note an apparent lower than catalogue polarization for VICyg 12 in other literature such as Simmons & Stewart (1985) and Arnold (2017). Thus, we believe it is more likely this behaviour is due to polarization variability in the source rather than an instrumental effect. In Table 2 we present the observed polarization degree compared to archival data.

Another way to estimate instrumental polarization is to check the distance between the origin and the red cross. From this analysis method we get $q_{inst} = 0.029$ and $u_{inst} = -0.019$ for VICyg 12 observations compared to $q_{inst} = 0.008$ and $u_{inst} = -0.021$ from unpolarized standard star BD +28 4211. We can see discrepancy in q_{inst} and u_{inst} between the two methods here, which we can see on the right-hand panel of Fig. 10. For shorter exposure time, we get $q_{inst} = 0.0183$ and $u_{inst} = -0.023$ for HD 204827 compared to $q_{inst} = 0.0157$ and $u_{inst} = -0.0211$ from unpolarized standard HD 212311. The match is better in this case and can be seen in left-hand panel of Fig. 11.

5.5 Effect of Cassegrain rotator angle

Finally, to characterize the instrument in more detail, we observed the three unpolarized and three polarized standard stars at different

Figure 8. Stokes q versus sequence of observed data for unpolarized standard stars BD +32 3739, BD +28 4211, and HD 212311 top, middle, and bottom panels, respectively, before we correct for instrumental polarization. The points represent data points from observation and the solid line represents the mean of the data points. The vertical line represents the error bar.
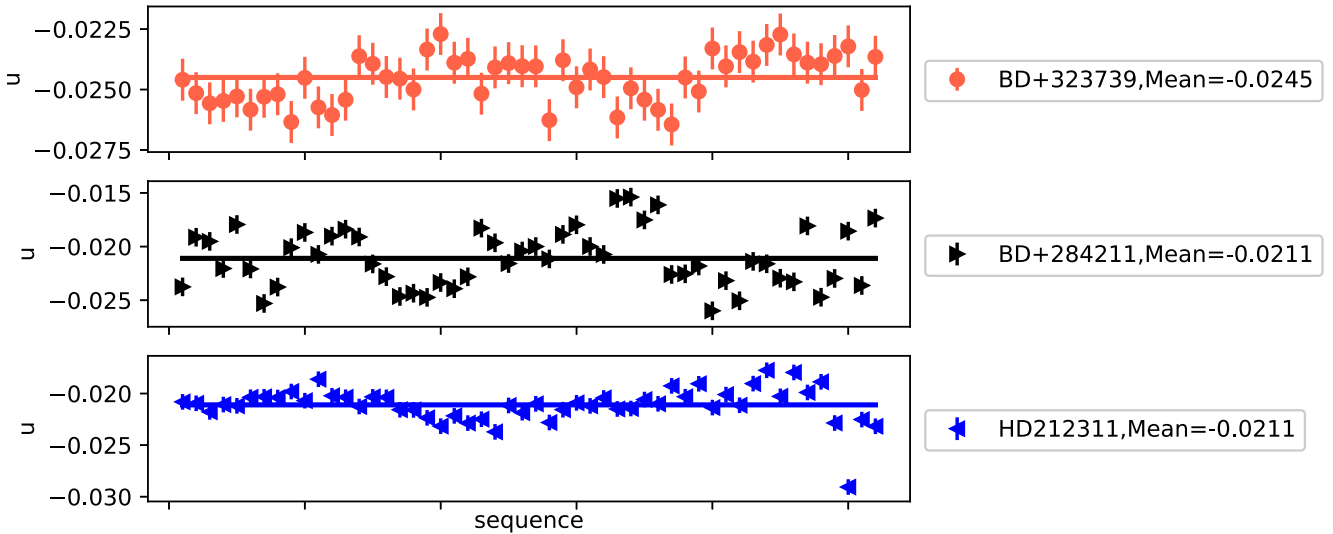

Figure 9. Stokes u versus sequence of observed data for unpolarized standard stars BD +32 3739, BD +28 4211, and HD 212311 from top, middle, and bottom panels, respectively before we correct for instrumental polarization. The points represent data points from observation and the solid line represents the mean of the data points. The vertical line represents the error bar.

Cassegrain rotor angles. We present results for three unpolarized standard stars BD+323739, BD+284211, and HD212311 in Figs 8 and 9 for observed Stokes *q* and *u* using two-camera technique. Mean values of these observations are presented in the label. We observed these stars at different Cassegrain rotor positions ranging from −90° to 90° with 22.5° intervals. In Figs 10 and 11 we present *q-u* plots for observed data before and after correcting for instrumental polarization, left and right, respectively for polarized standard stars VI-Cyg12 and HD 204827. We found that using the average of unpolarized standard star observations (with the same exposure time and Cassegrain rotor angle as the polarized standard observations) gave the best results. Hence, for future observations we recommend observing unpolarized standard stars with the same exposure time and Cassegrain rotor angles as science targets to estimate instrumental polarization.

6 CONCLUSIONS

In this paper, we have studied the performance of a prototype dual-beam, dual-camera polarimeter (MOPTOP) in laboratory testing and mounted on the Liverpool Telescope. We have described and tested a data reduction procedure that corrects for intrinsic sensitivity differences between each camera on a source-by-source basis. Analysis of observations shows that the technique of using two-cameras in a dual-beam polarimeter produces better polarization accuracy for the same exposure time as compared to a single-beam, single-camera polarimeter (such as RINGO3) as shown in Fig. 3 and lower error in polarization degree as shown in Fig. 5. There is better stability in the data from the two-camera technique compared to the one-camera technique as shown in Fig. 6 for all the targets observed on-sky. Thus, we recommend observers use the
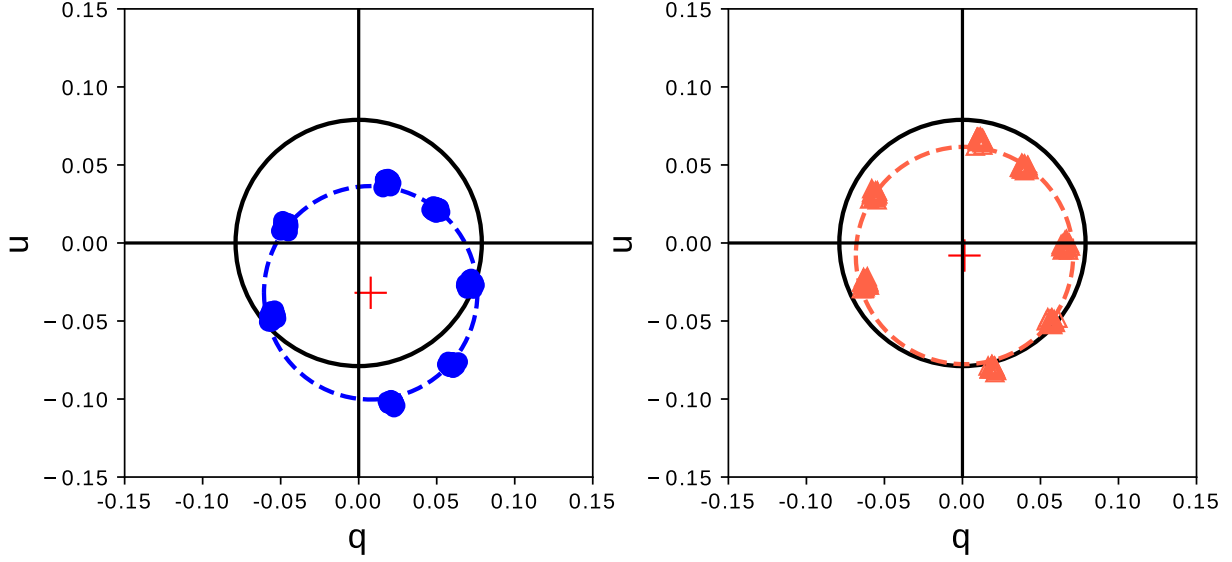
Figure 10. Stokes q versus Stokes u for polarized standard star VI-Cyg12 before correction for instrumental polarization on left and after correction for instrumental polarization on right. The red triangle and blue circle points represent the observed values for different Cassegrain rotor positions, dashed line is a best fit of the observed data, red cross represents the centre of the best fit, solid black lines represent the q=0 and u=0 lines for reference. And the solid black circle is the catalogue value of VICyg 12. Error bars are smaller than the points.
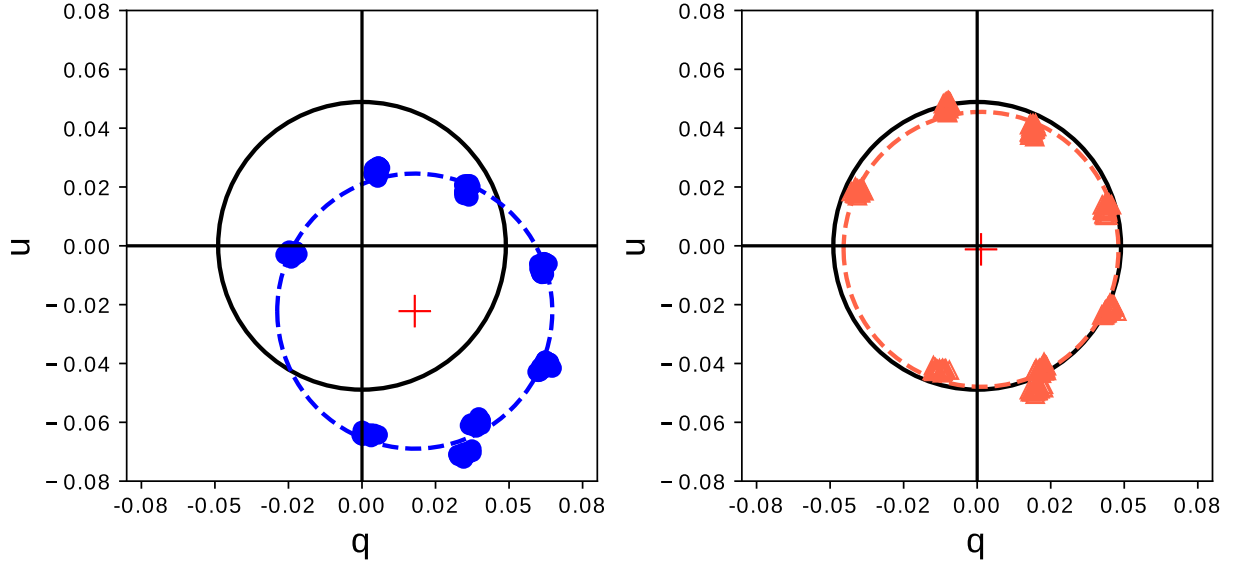
Figure 11. Stokes q versus Stokes u for polarized standard star HD 204827 before correction for instrumental polarization on left and after correction for instrumental polarization on right. The red triangle and blue circle points represent the observed values for different Cassegrain rotor positions, dashed line is a best fit of the observed data, red cross represents the centre of the best fit, solid black lines represent the $q = 0$ and $u = 0$ lines for reference. And the solid black circle is the catalogue value of HD 204827. Error bars are smaller than the points.

two-camera technique for the data reduction of future MOPTOP observations.

In lab data we find instrumental polarization < 0.25 per cent with a stability of ~ 0.05 per cent and a maximum degree of instrumental depolarization of < 5 per cent of the measured value. On-sky testing showed an instrumental polarization of 2.4 per cent caused by the telescope fold mirror with a stability of ~ 0.25 per cent.

In summary, we have shown observationally that a dual-beam polarimeter implemented using dual-cameras performs better than single beam methods. It also avoids the image overlap and sky noise issues of dual-beam, single camera polarimeters.

ACKNOWLEDGEMENTS

research. This research made use of PHOTUTILS, an Astropy package for detection and photometry of astronomical sources (Bradley et al. 2019).

REFERENCES

Arnold D., 2017, PhD thesis, Liverpool John Moores University
Boyajian T. S. et al., 2016, MNRAS, 457, 3988
Bradley L. et al., 2019, astropy/photutils: v0.6
Brown J. C., McLean I. S., 1977, A&A, 57, 141
Clarke D., 1965, MNRAS, 129, 71
Clarke D., Neumayer D., 2002, A&A, 383, 360
Cox L. J., 1976, MNRAS, 176, 525
Harvey E. J., Redman M. P., Darnley M. J., Williams S. C., Berdyugin A., Piirola V. E., Fitzgerald K. P., O'Connor E. G. P., 2018, A&A, 611, A3
Hoffman J. L., Leonard D. C., Chornock R., Filippenko A. V., Barth A. J., Matheson T., 2008, ApJ, 688, 1186
Jermak H., 2017, PhD thesis, Liverpool John Moores University
Jermak H. et al., 2016a, MNRAS, 462, 4267
Jermak H., Steele I. A., Smith R. J., 2016b, in Evans C. J., Simard L., Takami H., eds, Proc. SPIE Conf. Ser. Vol. 9908, Ground-based and Airborne Instrumentation for Astronomy VI. SPIE, Bellingham, p. 99084I
Jermak H., Steele I. A., Smith R. J., 2018, in Evans C. J., Simard L., Takami H., eds, Proc. SPIE Conf. Ser. Vol. 10702, Ground-based and Airborne Instrumentation for Astronomy VII. SPIE, Bellingham, p. 107024Q
Landolt A. U., 2009, AJ, 137, 4186
Mundell C. G. et al., 2013, Nature, 504, 119
Price-Whelan A. M. et al., 2018, AJ, 156, 18
Robbins M. S., Hadwen B. J., 2003, IEEE Trans. Electron Devices, 50, 1227
Scarrott S. M., Warren-Smith R. F., Pallister W. S., Axon D. J., Bingham R. G., 1983, MNRAS, 204, 1163
Schmidt G. D., Elston R., Lupie O. L., 1992, AJ, 104, 1563
Shrestha M., Neilson H. R., Hoffman J. L., Ignace R., 2018, MNRAS, 477, 1365
Simmons J. F. L., Stewart B. G., 1985, A&A, 142, 100
Słowikowska A., Krzeszowski K., Żejmo M., Reig P., Steele I., 2016, MNRAS, 458, 759
Steele I. A. et al., 2004, in Oschmann J. M.,ed., Proc. SPIE Conf. Ser. Vol. 9915, Ground-based Telescopes. SPIE, Bellingham, p. 679
Steele I. A., Mundell C. G., Smith R. J., Kobayashi S., Guidorzi C., 2009, Nature, 462, 767
Steele I. A., Jermak H., Copperwheat C. M., Smith R. J., Poshyachinda S., Soonthorntham B., 2016, in Holland A. D., Beletic J., eds, Proc. SPIE Conf. Ser. Vol. 9915, High Energy, Optical, and Infrared Detectors for Astronomy VII. SPIE, Bellingham,p. 991522
Steele I. A. et al., 2017, ApJ, 843, 143
Steele I. A., Copperwheat C. M., Jermak H. E., Kennedy G. M., Lamb G. P., 2018, MNRAS, 473, L26

This paper has been typeset from a TEX/LATEX file prepared by the author.